JOURNAL OF Applied Polymer SCIENCE

Special Issue: Polycarbonates and Green Chemistry

Guest Editors: Dr Sophie Guillaume (Université de Rennes 1) and Dr Laetitia Mespouille (University of Mons)

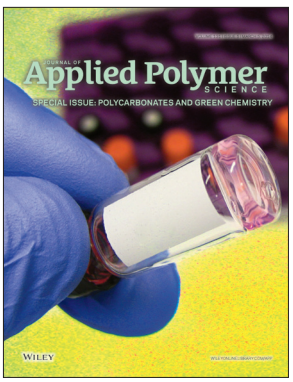

EDITORIAL

Polycarbonates and green chemistry
S. Guillaume and L. Mespouille, *J. Appl. Polym. Sci.* 2014, **DOI: 10.1002/app.40081**

REVIEWS

Porous crystals as active catalysts for the synthesis of cyclic carbonates
M. Zhu and M. A. Carreon, *J. Appl. Polym. Sci.* 2014, **DOI: 10.1002/app.39738**

Renaissance of aliphatic polycarbonates: New techniques and biomedical applications
J. Xu, E. Feng and J. Song, *J. Appl. Polym. Sci.* 2014, **DOI: 10.1002/app.39822**

RESEARCH ARTICLES

Chemical modification of bisphenol A polycarbonate by reactive blending with ethylene carbonate
M. Colonna, C. Berti and M. Fiorini, *J. Appl. Polym. Sci.* 2014, **DOI: 10.1002/app.39820**

Synthesis and characterization of poly(ester carbonate)s by melt-phase interchange reactions of dihydroxy compounds with alkylene and arylene diphenyl dicarbonates containing ester groups
B. A. Sweileh, H. R. Al-Qalawi and H. A. Mohammad, *J. Appl. Polym. Sci.* 2014, **DOI: 10.1002/app.39904**

Terpolymerization of benzyl glycidyl ether, propylene oxide, and CO_2 using binary and bifunctional [rac-SalcyCo^{III}X] complexes and the thermal and mechanical properties of the resultant poly(benzyl 1,2-glycerol-co-propylene carbonate)s and poly(1,2-glycerol-co-propylene carbonate)s
H. Zhang and M. W. Grinstaff, *J. Appl. Polym. Sci.* 2014, **DOI: 10.1002/app.39893**

Synthesis of biodegradable high molecular weight polycarbonates from 1,3-trimethylene carbonate and 2,2-dimethyltrimethylene carbonate
M. Pastusiak, P. Dobrzynski, J. Kasperczyk, A. Smola and H. Janecze, *J. Appl. Polym. Sci.* 2014, **DOI: 10.1002/app.40037**

Propylene carbonate as a source of carbonate units in the synthesis of elastomeric poly(carbonate–urethane)s and poly(ester–carbonate–urethane)s
M. M. Mazurek, P. G. Parzuchowski and G. Rokicki, *J. Appl. Polym. Sci.* 2014, **DOI: 10.1002/app.39764**

Synthesis and properties of biodegradable multiblock poly(ester-carbonate) comprising of poly(L-lactic acid) and poly(butylene carbonate) with hexamethylene diisocyanate as chain-extender
J. Wang, L. Zheng, C. Li, W. Zhu, D. Zhang, G. Guan and Y. Xiao, *J. Appl. Polym. Sci.* 2014, **DOI: 10.1002/app.39158**

Effect of interfacial tension on the cell structure of poly(methyl methacrylate)/bisphenol A polycarbonate blends foamed with CO_2
P. Gong and M. Ohshima, *J. Appl. Polym. Sci.* 2014, **DOI: 10.1002/app.39228**

Flame retardancy and thermal properties of carboxyl-containing polysiloxane derivatives in polycarbonate
R. Song, L. Chang and B. Li, *J. Appl. Polym. Sci.* 2014, **DOI: 10.1002/app.39814**

Clay-induced degradation during the melt reprocessing of waste polycarbonate
M. U. de la Orden, D. P. C. Muñoz, V. Lorenzo and J. M. Urreaga, *J. Appl. Polym. Sci.* 2014, **DOI: 10.1002/app.39997**

Preparation and properties of polycarbonate microspheres containing tetanus toxoid vaccine
B. Hu, X.-J. Ke, G.-P. Yan, R.-X. Zhuo, Y. Wu, C.-L. Fan and Y.-J. Liu, *J. Appl. Polym. Sci.* 2014, **DOI: 10.1002/app.40048**

New thermogelling poly(ether carbonate urethane)s based on pluronics F127 and poly(polytetrahydrofuran carbonate)
X. J. Loh, H. X. Gan, H. Wang, S. J. E. Tan, K. Y. Neoh, S. S. J. Tan, H. F. Diong, J. J. Kim, W. L. S. Lee, X. Fang, O. Cally, S. S. Yap, K. P. Liong and K. H. Chan, *J. Appl. Polym. Sci.* 2014, **DOI: 10.1002/app.39924**

Journal of Applied Polymer Science

Effect of Interfacial Tension on the Cell Structure of Poly(methyl methacrylate)/Bisphenol A Polycarbonate Blends Foamed with CO_2

Pengjian Gong, Masahiro Ohshima
Department of Chemical Engineering, Kyoto University, Kyoto 615-8510, Japan
Correspondence to: M. Ohshima (E - mail: oshima@cheme.kyoto-u.ac.jp)

ABSTRACT: A small amount of low-decomposition temperature poly(methyl methacrylate), (low-T_d PMMA), can be used as a compatibilizer for high-decomposition temperature PMMA (high-T_d PMMA) and polycarbonate (PC) blend systems. When low-T_d PMMA is thermally decomposed in the PMMA/PC blend, the PMMA-*g*-PC copolymer is formed. This copolymer decreases the interfacial tension between PMMA and PC, decreases the domain size of PC and increases the interfacial area. Blends of high-T_d PMMA/PC with different amounts of low-T_d PMMA undergo a batch physical foaming with CO_2. With increasing amounts of low-T_d PMMA, which is equivalent to increasing the PMMA-*g*-PC copolymer, the number density of bubbles increases due to the increase of the interfacial area of disperse domains. However, the interfacial tension is decreased and the heterogeneity of PMMA/PC blend is decreased with increasing amounts of the copolymer. The number of bubbles per unit interfacial area and that per unit number of domains are decreased.. © 2013 Wiley Periodicals, Inc. J. Appl. Polym. Sci. **2014**, *131*, 39228.

KEYWORDS: blends; copolymers; compatibilization; foams; surfaces and interfaces

Received 14 January 2013; accepted 25 February 2013
DOI: 10.1002/app.39228

INTRODUCTION

Polymeric foams are found in virtually every aspect of our daily lives, and they are used in a wide variety of applications, such as cushioning for furniture, food trays, packaging, thermal insulation materials, and in shock and sound attenuation materials.[1] The cell morphology of the foams, which is characterized by the cell density, cell size, and open and/or closed-cell structures, is selected based on the applications.[2] The desired cell morphology in the foams is prepared by selecting appropriate polymers, additives, fillers, processing schemes and tuning the processing conditions.

In polymer foaming processes, bubble nucleating agents such as talc or clay are often used to enhance the bubble nucleation and to improve the uniformity of the cell morphology. The nucleating agent increases heterogeneity in the polymer matrix and provides bubble nucleation sites with low activation energies where homogeneous bubble nucleation is significantly suppressed while heterogeneous bubble nucleation is enhanced.[3,4] The interfacial tension between the polymer matrix and the nucleating agent predominately determines the heterogeneous bubble nucleation and growth behaviors. Differences in the diffusivity and solubility of the foaming agent in the blend polymer could also be key factors for the heterogeneous nucleation of bubbles when disperse polymeric domains are used as bubble nucleating agents during the foaming of polymer blends.

A number of studies have been conducted on polymer blend foams where a minor polymer phase was used as a bubble nucleating agent and the relationship of the nucleation and growth of bubbles with the interfacial properties of the blended polymers was investigated. Sharudin et al. considered using a high interfacial tension polymer as a bubble nucleating agent and investigated the effect of the interfacial tension between polymers on bubble nucleation using polypropylene (PP)/polystyrene (PS) and PP/poly(methyl methacrylate) (PMMA) blends as example systems, where PP was used as a nucleating agent.[5] They conducted visual observation experiments, which revealed that the disperse PP domain acted as a bubble nucleating agent due to the higher interfacial tension between PP and PS as well as PMMA. During foam extrusion processes of pure low-density polyethylene (LDPE), microcellular foams could not be produced due to the high activation energy for bubble nucleation. Therefore, Park et al. blended PS with LDPE to induce heterogeneous bubble nucleation, which increased the cell density.[6] In addition to the immiscible polymer blends, block copolymer micelles were also investigated as an effective bubble nucleating agent. Siripurapu et al. reported that the cell density was significantly increased by adding CO_2-philic copolymers, PMMA-*g*-poly (dimethylsiloxane) (PDMS) and/or PMMA-*b*-poly (fluorooctyl methacrylate) (PFOMA), to a PMMA matrix.[7] However, Spitael et al. observed that the micelles formed by PS-*b*-poly

(ethylene propylene) (PEP) and/or PS-*b*-PMMA diblocks were not effective as bubble nucleating agents in a PS matrix.[8] It appears that the role of copolymer micelles is still ambiguous.

Compatibilizers are often used in polymer blends and composites to modify the interfacial properties and to increase the dispersibility of the minor phase in the matrix. Zhai et al. investigated the foaming behavior of PP/PS blends in which the PS-*g*-PP copolymer was used as a compatibilizer.[9] The authors reported that PS-*g*-PP copolymers with longer PS graft chains could improve the compatibility, and the copolymers decreased the domain size and lowered the CO_2 diffusion coefficient. The reduction of the domain size could increase the cell density. Ruckdaschel et al. reported a similar result in their foaming of poly(2,6-dimethyl-1,4-phenylene ether (PPE)/poly(styrene-*co*-acrylonitrile) (SAN) blends, in which the increase in the interfacial compatibility of the minor phase polymer could improve the dispersibility of the domains and increase the cell density.[10]

Reactive blending was conducted using diblock or graft copolymers to improve the interfacial properties of the minor and matrix phases and to produce well-dispersed polymer blends. Reactive blending is a unique and effective method for preparing a copolymer that has two distinct segments, typically a block or a graft copolymer, such that the copolymer can penetrate into both the matrix and disperse phases and modify the affinity between both phases.[11] In our previous study, reactive blending was utilized to form a polyethylene terephthalate (PET)-PC diblock copolymer, and we investigated the effects of the copolymer on the foaming behaviors of PET/PC blends.[12] It was observed that the PET-PC di-block copolymer increased the compatibility and enhanced the interfacial affinity.

For polymer blend foaming processes, the coalescence and aggregation of disperse domains results in less interfacial area and leads to a reduction in the number of bubble nucleation sites. Therefore, it is desirable to prevent the coalescence and aggregation of bubble nucleating agents, i.e., disperse polymer domains, and to uniformly disperse these nucleating agents as much as possible. To increase the dispersibility of the nucleating agents, the interfacial properties of the nucleating agents are modified and the heterogeneity of the nucleating agents is reduced through modifications of their surfaces or interfaces. These modifications might depress the heterogeneous bubble nucleation rate because when the interfacial tension between blended polymers is less than the surface tensions between the polymers and foaming gas, the energy required for bubble nucleation at the interface becomes high. This competitive effect of surface (interface) modification of bubble nucleating agents, i.e., minor polymer phase, has not yet been quantitatively investigated, although several studies have been reported on successful improvements of the cellular structure by controlling the affinity of the disperse domain with the use of compatibilizers, as mentioned above.

In this study, the CO_2 foaming behavior of a polymer blend, PMMA/PC blend, with a compatibilizer was investigated to determine the effect of interfacial tension between disperse and matrix polymers on bubble nucleation. The copolymer was produced in the PMMA/PC blend through reactive blending and was used as the compatibilizer. PMMA/PC blends have been extensively studied, particularly in terms of the miscibility of the blend.[13–17] The thermal degradation of PMMA occurs at approximately 240°C and produces macro-radicals, which could react with the molecular chains of PC to form a graft copolymer in the PMMA/PC blend. The graft copolymer subsequently increases the miscibility between the PMMA and PC phases.[18] Cole et al. reported that the adhesiveness of the PMMA-PC interface prepared by high-temperature melt blending (reactive blending) was six times greater than that prepared by solvent blending due to the formation of the graft copolymer.[19] The authors concluded that the thermal degradation reaction provides a unique route to improve the miscibility of the system. We used a grade of PMMA where the thermal degradation temperature was low (low-T_d PMMA) to produce the copolymer, and used the copolymer as a compatibilizer during the reactive processing of a high-thermal degradation temperature PMMA (high-T_d PMMA) and PC blend. The Palierne model was applied to calculate the interfacial tension between the domain and matrix polymers in the blend prepared through the reactive blending of PMMA/PC with the low-T_d PMMA. By observing the number density of the cell, the number density of the domain and the bubble as well as domain sizes from SEM micrographs of the blend foams, the number of bubbles per unit interfacial area and that of per unit number of domains were calculated to quantitatively determine the effect of interfacial tension on bubble nucleation.

EXPERIMENTAL

Materials

PC (Taflon A2600, M_w = 32,000 g mol^{-1}, Idemitsu Kosan, Japan), which had a density of 1.2 g cm^{-3} and a melt flow index of 6 g/10 min (300°C, 1.2 kg), and a high-thermal degradation temperature PMMA (high-T_d PMMA; SUMIPEX LG, M_w = 123,000 g mol^{-1}, Sumitomo Chemical, Japan), which had a density of 1.18 g cm^{-3}, a melt flow index of 10 g/10 min (230°C, 3.8 kg) and a thermal decomposition temperature, T_d, of 314°C (2% weight loss at 10°C min^{-1} in a nitrogen atmosphere), were used as the disperse domain and matrix polymers, respectively. The low-thermal degradation temperature PMMA (low-T_d, PMMA; M_w = 120,000 g mol^{-1}, Aldrich Chemistry, Japan), which had a T_d of 240°C (2% weight loss at 10°C min^{-1} in a nitrogen atmosphere), was used to form a copolymer and make the high-T_d PMMA compatible with PC. Isotactic PP (i-PP; Prime polymer F133A) with a 97% tacticity and a melt flow index of 3 g/10 min (230°C, 2.16 kg) was used as a disperse polymer in a reference blend system. i-PP has a melting temperature of 167°C, and its crystallinity is 57.5%. All the polymers were used as received. The glass transition temperatures (T_g) of the low-T_d and high-T_d PMMA are 96°C and 103°C, respectively. The T_g of PC is 151°C. CO_2 (99.95% pure) (Showa-Tansan, Japan) was used as a physical foaming agent.

Preparation of the PMMA/PC and PMMA/PP Blends

Both high-T_d and low-T_d PMMA and PC pellets were dried at 70°C in a temperature-controlled oven for at least 2 days to remove moisture before blending. Pellets of the low-T_d PMMA and PC were first dry-mixed at three different weight ratios of

Table I. Weight Ratio of PMMA/PC Blends

Component	high-T_d PMMA/low-T_d PMMA/PC		
Sample no.	1	2	3
PMMA/PC 90/10	90/0/10	89.5/0.5/10	89/1/10
PMMA/PC 70/30	70/0/30	68.5/1.5/30	67/3/30

low-T_d PMMA to PC, 0/100, 5/95 and 10/90. These mixtures were fed into a melt-mixer (Labo Plastomill, 4C150 Toyoseiki, Japan) to reactively blend at 240°C. The reactive blending was conducted for 30 min to ensure that the low-T_d PMMA fully reacted with the PC. The obtained samples were subsequently mixed with the high-T_d PMMA using the same melt-mixer at 240°C for 10 min to prepare the PMMA/PC blend. The PMMA/PC blends were prepared with two different weight ratios of the low-T_d and high-T_d PMMA to PC, 90/10 and 70/30. The detailed weight ratios of the low-T_d and high-T_d PMMA to PC in the blends are summarized in Table I.

A high-T_d PMMA and PP blend was prepared as a reference system. The PMMA/PP blend with a 70/30 weight ratio exhibited a co-continuous phase morphology. Therefore, only the 90/10 PMMA/PP blend was prepared by melt-blending for 10 min at 220°C in the same mixer and used as the reference system.

Reactive blending and melt-blending were conducted by rotating a kneading rotor at 10 rpm for the first 2 min, and then the rotation speed was increased to 50 rpm for the remaining time. After blending, the blends were molded into the plate-shape of 35 mm in width, 60 mm in length and 1 mm in thickness using a hot compression molding machine. The copolymer, which was generated by the reaction between low-T_d PMMA and PC, was extracted using a selective solvent (acetone) for PMMA, and the soluble fraction was analyzed by infrared spectroscopy.[15]

CO_2 Foaming

All the blends were placed into a high pressure autoclave to dissolve CO_2 at 10 MPa under three different sorption and foaming temperatures, 60, 80, and 100°C. After saturating the blends with CO_2 for 22 h, the pressure in the autoclave was released within 2 s to induce foaming. The sorption time of 22 h was fixed for all experiments to ensure the same equilibrium state.

Measurements of PMMA/PC Blends Reaction

A thermogravimetric analyzer (TGA: DTG-60H, Shimadzu, Japan) was used to determine the thermal degradation temperatures of the high and low-T_d PMMA from the weight loss measured during heating. PMMA was heated from 40 to 240°C at a rate of 10°C min^{-1} and held at 240°C for 60 min. At 240°C, reactive or melt-blending occurred. The entire process was conducted under a nitrogen purge at a flow rate of 50 mL min^{-1}. A differential scanning calorimeter (DSC: Pyris 1 Perkin Elmer) was used to measure the T_g. The samples were heated from 40 to 260°C at a rate of 10°C min^{-1}, held at that temperature for 5 min and then cooled to 40°C. The first scan was performed to remove the thermal history, and the T_g was therefore determined from the second scan. The rheological properties were measured using a rheometer (Advanced Rheometric Expansion System, ARES, TA Instruments) to observe the changes in the rheological properties of the PMMA/PP and PMMA/PC blends. Parallel plate geometry was used for the dynamic frequency sweep tests at 240°C for the PMMA/PC blends and at 220°C for the PMMA/PP blend in the frequency range of 0.01 to 100 rad/s. Gap of 1 mm and strains of 10 to 15% were applied during the measurements. A strain sweep test was also conducted to determine the strain limit for a linear viscoelastic response. The phase angle was checked at lower frequencies to avoid inaccurate data where the phase angle was too close to 90°.[20] Fourier transform infrared spectroscopy (FT-IR: VERTEX 70, Bruker Optik GMBH, Germany) was used to investigate the characteristic chemical groups in the PMMA/PC blends in the range of 400 to 4000 cm^{-1} at a resolution of 4 cm^{-1}. The film of soluble fractions was prepared by solvent evaporation before the measurement.

Characterization of Blend and Foam Morphology

Scanning electron microscopy (SEM) was used to observe the blend and cell morphology of the foam. The samples were frozen in liquid nitrogen to create cryogenic fractural surfaces and then coated with gold for 180 s before observation under a SEM (Tiny-SEM 1540, Technex Co. Ltd., Japan) or field emission SEM (JSM-6700F, Jeol, Japan). FESEM (JSM-6700F) images were collected at an acceleration voltage of 10 kV, a current of 5 μA and a wide distance of 8 mm. The image processing software ImageJ was used to calculate the disperse domain density, N_d, and the number average domain radius, $\overline{R_d}$, from the SEM micrographs.

$$\overline{R_d} = \frac{1}{c}\sum_i^c R_i \tag{1}$$

$$N_d = \frac{\phi}{\overline{V_c}} = \frac{\phi}{\frac{4}{3c}\pi\sum_i^c R_i^3} \tag{2}$$

where R_i is the radius of the i-th domain measured from the SEM micrographs. $\overline{R_d}$ is calculated by averaging the domain radii. ϕ is the volume fraction of the disperse domain, and it is calculated from the weight ratios and densities of both polymers.

The interfacial area between the disperse domain and matrix per unit volume of blend, S, is calculated by:

$$S = N_d\overline{S_c} = N_d\frac{4}{c}\pi\sum_i^c R_i^2 \tag{3}$$

where $\overline{S_c}$ is the number average domain surface.

The cell density, N_f, and the number average cell radius, $\overline{R_n}$, were also calculated from the SEM micrographs. The bulk densities of the samples before and after foaming were measured using a densitometer (Mirage Electronic Densimeter MD-200S) and used for the cell density calculation. The cell density was then calculated by:[21]

$$N_f = \frac{\rho_f}{\rho_s} \times \left(\frac{n}{A}\right)^{1.5} \tag{4}$$

where n is the number of bubbles in a total area A. ρ_f and ρ_s are the densities of the foam and solid bulk, respectively.

The number of observable bubbles per unit interfacial area, D_s, and the number of observable bubbles per unit number of domains, D_d, were calculated by

$$D_s = N_f/S \tag{5}$$

$$D_d = N_f/N_d \tag{6}$$

THEORY OF BLEND CHARACTERIZATION IN BRIEF

Component Fraction from the Fox Equation

The T_g of a miscible polymer blend is estimated through the Fox equation. When this equation is applied to partially miscible polymer blends to calculate the composition of each phase, it is common to assume that the minor polymer is homogeneously infused in the major polymer phase. We applied the Fox equation to the PMMA/PC blend to estimate the weight fraction of PMMA infused in the PC domain and that of PC infused in the PMMA matrix.[22,23]

$$\frac{1}{T_g'} = \frac{\omega'_{PMMA}}{T_{gPMMA}} + \frac{\omega'_{PC}}{T_{gPC}} \tag{7}$$

and

$$\frac{1}{T_g''} = \frac{\omega''_{PMMA}}{T_{gPMMA}} + \frac{\omega''_{PC}}{T_{gPC}} \tag{8}$$

where ω'_{PC} is the weight fraction of PC infused in the PMMA-matrix, ω'_{PMMA} $(1 - \omega''_{PC})$ is the weight fraction of PMMA in the PMMA-matrix, ω''_{PMMA} $(1 - \omega''_{PC})$ is the weight fraction of PMMA in the PC-domain, ω''_{PC} is the PC weight fraction in the PC-domain, T_g' is the glass transition temperature of the PMMA-matrix, T_g'' is the glass transition temperature of the PC-domain, T_{gPMMA} is the glass transition temperature of the pure PMMA and T_{gPC} is the glass transition temperature of the pure PC.

The weight fractions of PC in the PMMA matrix and that of PMMA in the PC domain were calculated using eqs. (9) and (10) with the T_g data of blend and neat polymers.

$$\omega'_{PC} = \frac{T_{gPC}(T_{gPMMA} - T_g')}{T_g'(T_{gPMMA} - T_{gPC})} = 1 - \omega'_{PMMA} \tag{9}$$

and

$$\omega''_{PMMA} = \frac{T_{gPMMA}(T_{gPC} - T_g'')}{T_g''(T_{gPC} - T_{gPMMA})} = 1 - \omega''_{PC} \tag{10}$$

Furthermore, the weight fractions of both the PC domain and the PMMA matrix could be calculated from mass balances by transforming eqs. (9) and (10)

$$\omega' = \frac{\omega_{PC} - \omega''_{PC}}{\omega'_{PC} - \omega''_{PC}} \tag{11}$$

and

$$\omega'' = \frac{\omega_{PC} - \omega'_{PC}}{\omega''_{PC} - \omega'_{PC}} \tag{12}$$

where ω' is the estimated weight fraction of the PMMA matrix, ω'' is the estimated weight fraction of the PC domain in the blend after reactive blending, and ω_{PC} is the PC domain weight fraction (10% or 30%) in the blend before reactive blending.[22,23]

Estimate of Interfacial Tension

A sea-island structure is frequently observed in immiscible polymer blends after blending. In the blending process, the morphology evolution consists of stretching the fluid droplet into threads, the break-up of the threads into smaller droplets and the coalescence of the droplets into larger domains.[11] The ultimate domain diameter is related to the force balance, which is a function of the interfacial tension between two components, the viscosity ratio, and the shear stress. Palierne has reported a theory for concentrated emulsions with a viscoelastic constituent.[24] This theory can be applied to polymer blends, which go through dynamic shear with very small drop deformation from a spherical shape; the geometrical relaxation of the disperse domain would lead to a long relaxation process during the dynamic moduli test in the low frequency region.[25] The storage modulus at the relaxation process, i.e., the G' at the secondary plateau, is directly related to the interfacial tension between the disperse domain and the matrix.[26] The Palierne model, which accounts for the viscoelastic nature of the component phases and the particle size distribution in non-dilute emulsions, exhibits a relationship among the complex shear modulus, blend morphology and interfacial tension:[20]

$$G^* = G_m^*\left[\frac{1 + 3/2\sum_i \frac{\phi_i E_i}{D_i}}{1 - \sum_i \frac{\phi_i E_i}{D_i}}\right] \tag{13}$$

$$E_i = 2(G_d^* - G_m^*)(19G_d^* + 16G_m^*) + \frac{48\beta_d^*\Gamma^0}{R_i^2} + \frac{32\beta_s^*(\Gamma^0 + \beta_d^*)}{R_i^2} + \frac{8\Gamma^0}{R_i}(5G_d^* + 2G_m^*) + \frac{2\beta_d^*}{R_i}(23G_d^* - 16G_m^*) + \frac{4\beta_s^*}{R_i}(13G_d^* + 8G_m^*) \tag{14}$$

and

$$D_i = (2G_d^* + 3G_m^*)(19G_d^* + 16G_m^*) + \frac{48\beta_d^*\Gamma^0}{R_i^2} + \frac{32\beta_s^*(\Gamma^0 + \beta_d^*)}{R_i^2} + \frac{40\Gamma^0}{R_i}(G_d^* + G_m^*) + \frac{2\beta_d^*}{R_i}(23G_d^* + 32G_m^*) + \frac{4\beta_s^*}{R_i}(13G_d^* + 12G_m^*) \tag{15}$$

where Γ^0 is the interfacial tension. G_d^*, G_m^*, and G^* are the complex moduli of the disperse domain, matrix and emulsion in a range of frequencies, respectively. ϕ_i is the volume fraction of a domain with a radius R_i. β_d^* is the surface dilatation modulus associated with area variations, and β_s^* is the surface shear

modulus attributed to the resistance of the interface to shear deformation. Both of the complex moduli are frequency dependent.

β_d^* is usually associated with the non-uniformity of the interface, and β_s^* is associated with the resistance to shear deformation. It is assumed that, in the melt blends of this study, the interface is uniformly occupied by the copolymer such that the surface dilatation modulus can be ignored. However, due to the shear deformation resistance of the copolymer, β_s^* should be expressed by:[20]

$$\beta_s^* = \beta_s' + \beta_s'' \tag{16}$$

for $\omega\lambda_\beta < 1$:

$$\beta_s' = \beta_0 \tag{17}$$

$$\beta_s'' = \beta_0 \omega\lambda_\beta \tag{18}$$

for $\omega\lambda_\beta > 1$:

$$\beta_s' = \beta_s'' = \beta_0\sqrt{\omega\lambda_\beta} \tag{19}$$

where β_0 is a low-frequency plateau in the storage modulus for the copolymer and λ_β is a characteristic relaxation time.

ϕ_i and R_i were calculated from the SEM micrographs of the blend morphology. G_d^* and G_m^* were determined by individually measuring the complex moduli of the neat polymers. Then, Γ^0 and β_0 were determined such that the complex moduli estimated by the model could fit the experimental data. The detailed procedure for calculating the interfacial tension can be found elsewhere.[20]

Heterogeneous Bubble Nucleation at the Interface

The heterogeneous bubble nucleation rate (J) induced by a pressure quench can be expressed by the following equations:[27]

$$J = N^{2/3}\left(\frac{1-m_A}{2}\right)\left(\frac{2\gamma_A}{\pi mBF}\right)^{1/2}\exp\left[\frac{-16\pi\gamma_A^3 F}{3kT_{sys}(P_{bub,cr}-P_{sys})^2}\right] \tag{20}$$

where

$$F = \frac{1}{4\gamma_A^3}\left[\gamma_A^3\left(2-3m_A+m_A^3\right)+\gamma_B^3\left(2-3m_B+m_B^3\right)\right] \tag{21}$$

$$m_A = \cos\theta = \frac{\gamma_A^2+\gamma_{AB}^2-\gamma_B^2}{2\gamma_A\gamma_{AB}} \tag{22}$$

$$m_B = \cos\varphi = \frac{\gamma_B^2+\gamma_{AB}^2-\gamma_A^2}{2\gamma_B\gamma_{AB}} \tag{23}$$

γ_A, γ_B, and γ_{AB} represent the surface tension between polymer A and the blowing agent (CO_2), polymer B and CO_2, and the interfacial tension between polymer A and polymer B, respectively. N is the number density of the dissolved blowing agent molecules. $P_{bub,cr}$ is the pressure in a critical bubble, and P_{sys} is the system pressure. k is the Boltzmann constant, and T_{sys} is the system temperature. In the CO_2 foaming process, m, which is the molecular mass of gas molecules, is 44 g mol^{-1}, and B is normally approximated to be 2/3. θ and φ are the angles of γ_A with γ_{AB} and γ_B with γ_{AB}, respectively.

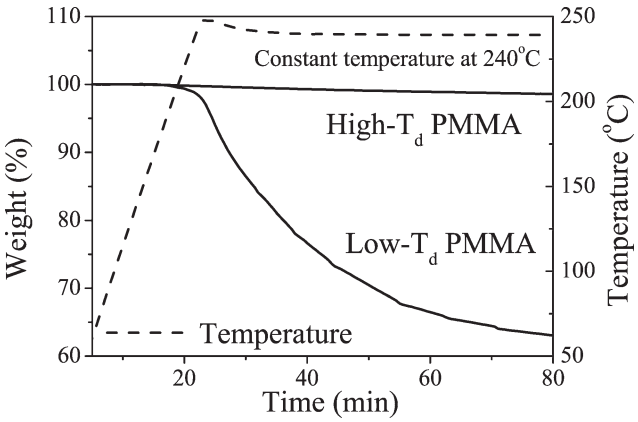

Figure 1. TGA curves of high-T_d and low-T_d PMMA.

RESULTS AND DISCUSSION

Characterization of Blend Properties

Because PP is immiscible and did not react with PMMA, only the PMMA/PC blends were characterized using TGA, DSC, and FT-IR. The thermal stabilities of the high-T_d PMMA and low-T_d PMMA were analyzed using TGA, and the results are shown in Figure 1. Note that the high-T_d PMMA exhibited a very small degradation with less than a 2% weight loss. However, the degradation of low-T_d PMMA began a weight loss at 200°C and a knee-point appeared in the weight-time curve at approximately 240°C. At the end of the TGA measurement, 37% of the low-T_d PMMA proceeded through the thermal degradation reaction. In our experiment, it was observed that a mixing time of 40 min was sufficient to complete the grafting reaction between the low-T_d PMMA and PC.

During the thermal degradation reaction between the low-T_d PMMA and PC, a graft copolymer was generated. This copolymer exhibits the same peaks as PMMA and PC in the FT-IR spectra, which makes identifying the occurrence of a grafting reaction difficult. The selective solvent extraction method was employed to overcome this difficulty, where a PMMA-rich phase is selectively dissolved in acetone. The PC-rich phase remained as the non-soluble residues.[28,29] Because PC molecules were chemically connected to PMMA in the form of a copolymer and infused in the PMMA-rich phase, the PC chain segments should be detected in the PMMA-rich phase and extracted along with the PMMA molecules in acetone. When the extracted phase, which is the PMMA-rich phase, is analyzed by FT-IR, the carbonyl stretching band of the PC carbonate group at 1773 cm^{-1} and that of the PMMA ester group at 1733 cm^{-1} may appear in the spectra. However, the presence of the 1773 cm^{-1} band might be superposed by the 1733 cm^{-1} band or the peak would be too small to be detected. In our study, Debier's strategy was employed to overcome the aforementioned problem.[29] Figure 2 presents the FT-IR spectra of the 70/30 (PMMA/PC) blends extracted in acetone. Two characteristic

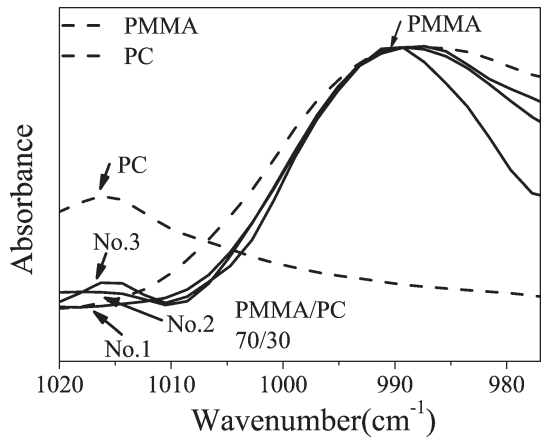

Figure 2. FT-IR spectra of PC, PMMA, and 70/30 wt % PMMA/PC blends (no. 1, 2. and 3).

peaks appeared in the spectra, which are very important for identifying the existence of the copolymer: (1) 1017 cm^{-1}, the vibration from a para-disubstituted benzene ring in PC and (2) 990 cm^{-1}, the vibration of the hydrocarbon bond in PMMA. The emergence of a peak at 1017 cm^{-1} and the increase in the height of the peak with the increasing amount of low-T_d PMMA indicated that sample blends No. 2 and 3 in Table I were partially miscible. For the 70/30 weight ratio blend (sample No. 1), the amount of copolymer dissolved in acetone may have been too small to be detected.

With the presence of the copolymer, the miscibility of the high-T_d PMMA and PC increased and the T_g of both PMMA and PC became closer to each other. Figure 3 presents the DSC curves of the 70/30 (PMMA/PC) blends with different weight ratios of low-T_d PMMA in the blend. Because PMMA and PC were not completely miscible, two T_g peaks clearly appeared in the heating curves of the blend samples. However, the T_g of PC (PC-disperse domain), which is denoted by T_g'', decreased from 151 to 138°C, and the T_g of PMMA (PMMA matrix), T_g', increased from 96 to 99.9°C as the low-T_d PMMA ratio increased.

With the assumption that the PMMA segment in the copolymer was homogeneously infused into the PC domain and a miscible state was achieved in both the domain and matrix, the Fox equation was applied to the DSC data and the weight fraction of PMMA infusing into the disperse PC domain and that of the PC infusing into the PMMA matrix was estimated using eqs. (9) and (10). The results of these estimates are presented in Table II. The details of the calculations are given elsewhere.[30,23] Although the thermal degradation of the high-T_d PMMA is difficult, it appears to have some capability of generating copolymers through the degradation reaction: 9% PC in the PMMA matrix and 8% PMMA in the disperse PC domain in 70/30 were estimated in sample no. 1, where no low-T_d PMMA was used. As the ratio of low-T_d PMMA increased, the weight percentage of PMMA infused in the PC domain increased to 16% in sample no. 3 of the 70/30 blend.

Figure 4 presents the SEM micrographs of the morphologies of the PMMA/PC (70/30 and 90/10) and PMMA/PP 90/10 blends. The sea-island morphology was observed in all the blends. The disperse domain was PP or PC, whereas the matrix was PMMA. Because the PMMA/PC blends were prepared by reactive blending, the domain size of PC was considerably smaller than the PP domain. As can be seen in the DSC data of samples no. 1 to no. 3, a higher amount of low-T_d PMMA would produce considerably more graft copolymer and increase the miscibility between the PC domain and PMMA matrix. Consequently, the diameter of the domain decreased. This increase in miscibility was also observed in the SEM micrographs presented in Figure 4. Cavities or voids were observed in the PMMA/PP and PMMA/PC no. 1 blends. These morphological features were produced due to detachment of the PP or PC domain from the PMMA matrix when we cut the samples for SEM observation. The number of cavities or voids became insignificant as the amount of lower-T_d PMMA increased.

Characterization of Interfacial Tension

The storage modulus, G', of the PMMA/PC blends is shown in Figure 5. The viscoelastic modulus in un-crosslinked amorphous polymers over a broad range of frequencies normally starts from the glassy zone, across a transition zone to a plateau zone, and finally to the terminal zone. In our study, the pure PMMA and PC polymers were already in the terminal zone at 240°C, where both the storage modulus and loss modulus decreased with decreasing frequency. When the frequency was less than 0.25 rad s^{-1}, the storage modulus, G', of PMMA was too small to be accurately measured. The G' of PC also exhibited an erroneous value at frequencies less than 0.063 rad s^{-1}. The immiscible characteristic of the PMMA/PP blend produced a less distinct plateau region; therefore, it was not included in Figure 5. For the PMMA/PC blends, a plateau region emerged in the frequency range from 1 to 0.063 rad s^{-1}. The plateau at lower frequencies was attributed to the relaxation of the disperse domain, whereas the plateau at higher frequencies was attributed to the relaxation of the matrix.[26] Here, the secondary plateau is highlighted because it is directly related to the interfacial tension. When the interfacial tension decreases, the domain size decreases and the total interfacial area increases. The former

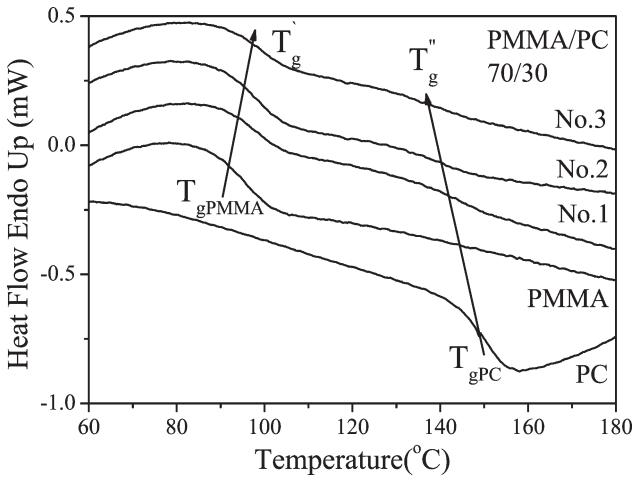

Figure 3. DSC heating curves of PC, PMMA, and 70/30 wt % PMMA/PC blends (no. 1, 2, and 3).

Table II. T_g and the Estimated Weight Percentage of PMMA and PC Composition in the PMMA-Matrix and PC-Domain of the PMMA/PC Blends

	PMMA matrix				PC domain			
PMMA/PC	T_g''(°C)	ω''_{PMMA}(%)	ω''_{PC}(%)	ω''(%)	T_g''(°C)	ω''_{PMMA}(%)	ω''_{PC}(%)	ω''(%)
70/30								
No. 1	98.8	91	9	74	144	8	92	26
No. 2	99.0	91	9	73	140	13	87	27
No. 3	99.9	88	12	75	138	16	84	25
90/10								
No. 1	97.2	96	4	93	145	7	93	7
No. 2	97.3	95	5	93	140	13	87	7
No. 3	97.6	95	5	94	137	18	82	6

effect shifts the interfacial contribution to higher frequencies, whereas the latter increases its modulus.[31] With the increase of copolymer, the plateau was shifted to a higher position, as shown in Figure 5 where the plateau changes from 0.4 rad s^{-1} in sample no. 1 with a 70/30 ratio to 1 rad s^{-1} in sample no. 3 with the same ratio. The magnitude of the plateau also increased to a higher modulus, as shown in the enlarged figure in lower right corner.

The measured domain size was subsequently used to calculate the interfacial tension of the PMMA/PP and PMMA/PC blends through the Palierne model, eqs. (13) to (19). The calculated interfacial tensions are provided in Table III. The interfacial tension was determined to fit the experimentally obtained storage modulus and loss modulus curves with the model. Figure 6 presents the experimental data for both the storage and loss modulus curves and the model estimate for both the PMMA/PC and PMMA/PP blends. The Palierne model provided a good agreement with the experimental data at frequencies greater than 0.25 rad s^{-1}. Specifically, the location and the magnitude of the secondary plateau were precisely expressed by the model. Some fitting error at low frequencies was most likely due to the inaccurate measurement of the storage modulus of PMMA.

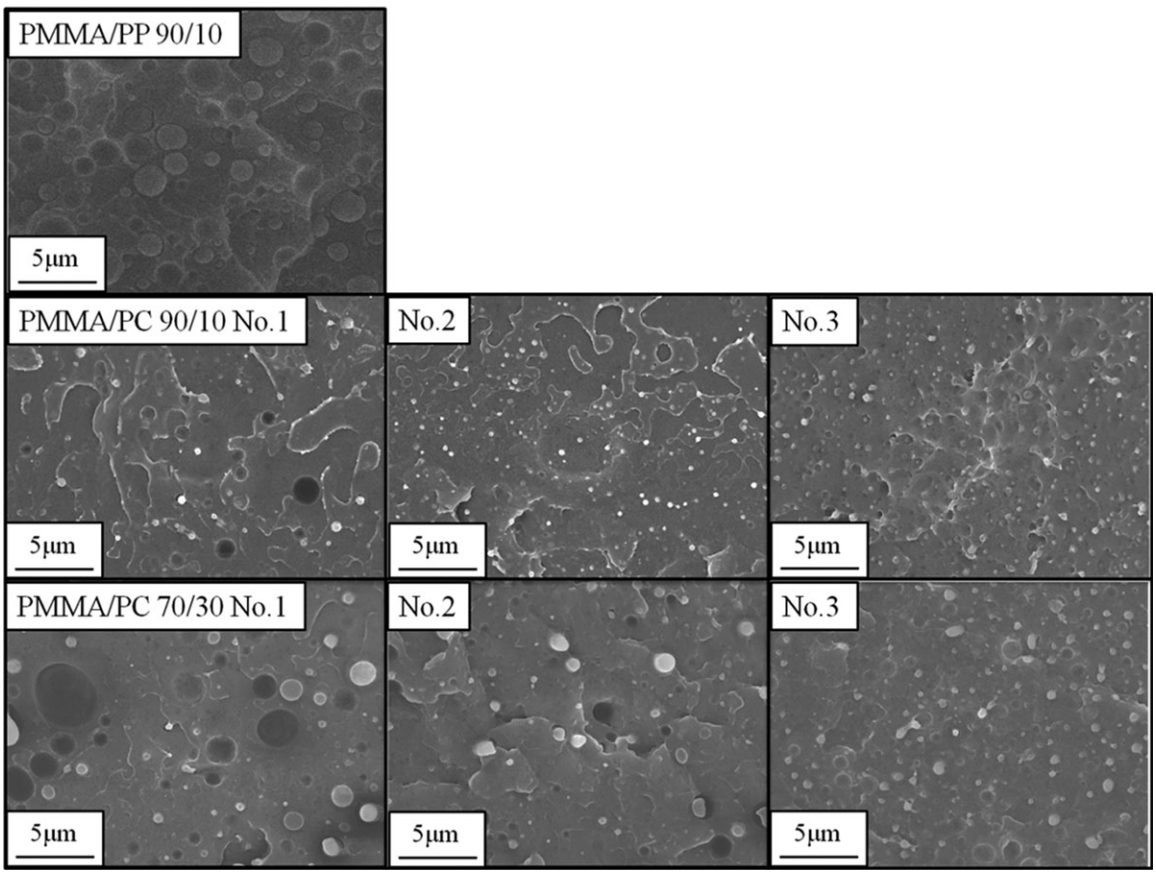

Figure 4. The morphologies of the 90/10 wt % PMMA/PP and the 70/30 wt % and 90/10 wt % PMMA/PC blends (no. 1, 2, and 3).

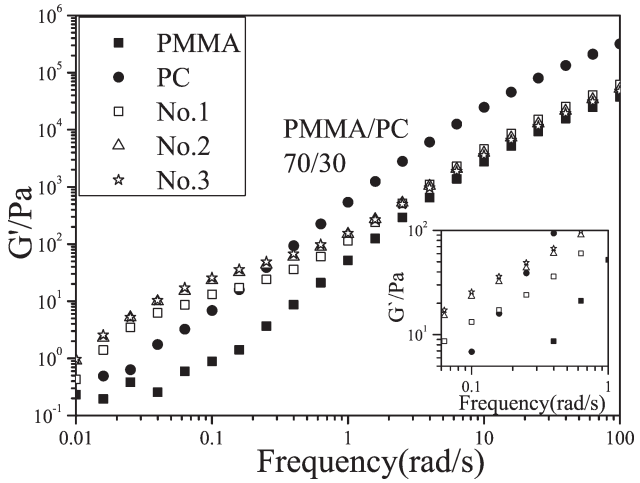

Figure 5. Comparison of the dynamic storage modulus curves, *G*, of PC, PMMA, and 70/30 wt % PMMA/PC blends (no. 1, 2, and 3).

Note that the PMMA/PP blend exhibited the greatest interfacial tension of 4.7 mN m^{-1} and the PMMA/PC blends exhibited less interfacial tension, which decreased in both the 70/30 and 90/10 blends as the amount of low-T_d PMMA was increased.

For polymer blends, the interfacial tensions have been reported to be rather small values of approximately 1 to 10 mN m^{-1}.[31] In the case of polymer blends prepared by reactive blending, the value of interfacial tension might be even smaller. The nonreactive nylon/rubber blend had an interfacial tension as high as 9 mN m^{-1}, whereas the reactive nylon/rubber blend was on 0.25 mN m^{-1}.[32] Virgilio et al. used the breaking thread method and measured the interfacial tension of PMMA with PP to be 5 mN m^{-1}.[33] Moussaif and Jerome employed the imbedded fiber retraction method and measured the interfacial tension of PMMA with PC to be 0.6 mN m^{-1}.[34] The interfacial tension calculated in this study was quite close to these reported values.

Table III. Interfacial Tension Calculated Using the Palierne Model

Blend component	Interfacial tension (mN/m)
PMMA/PP 90/10	4.7
PMMA/PC 70/30	
No. 1	0.76
No. 2	0.63
No. 3	0.51
PMMA/PC 90/10	
No. 1	0.47
No. 2	0.41
No. 3	0.37

The domain diameter, $2 \times \overline{R_d}$, and the interfacial area per unit blend volume, *S*, for the PMMA/PC and PMMA/PP blends were then calculated using eqs. (1) to (3), and the data were

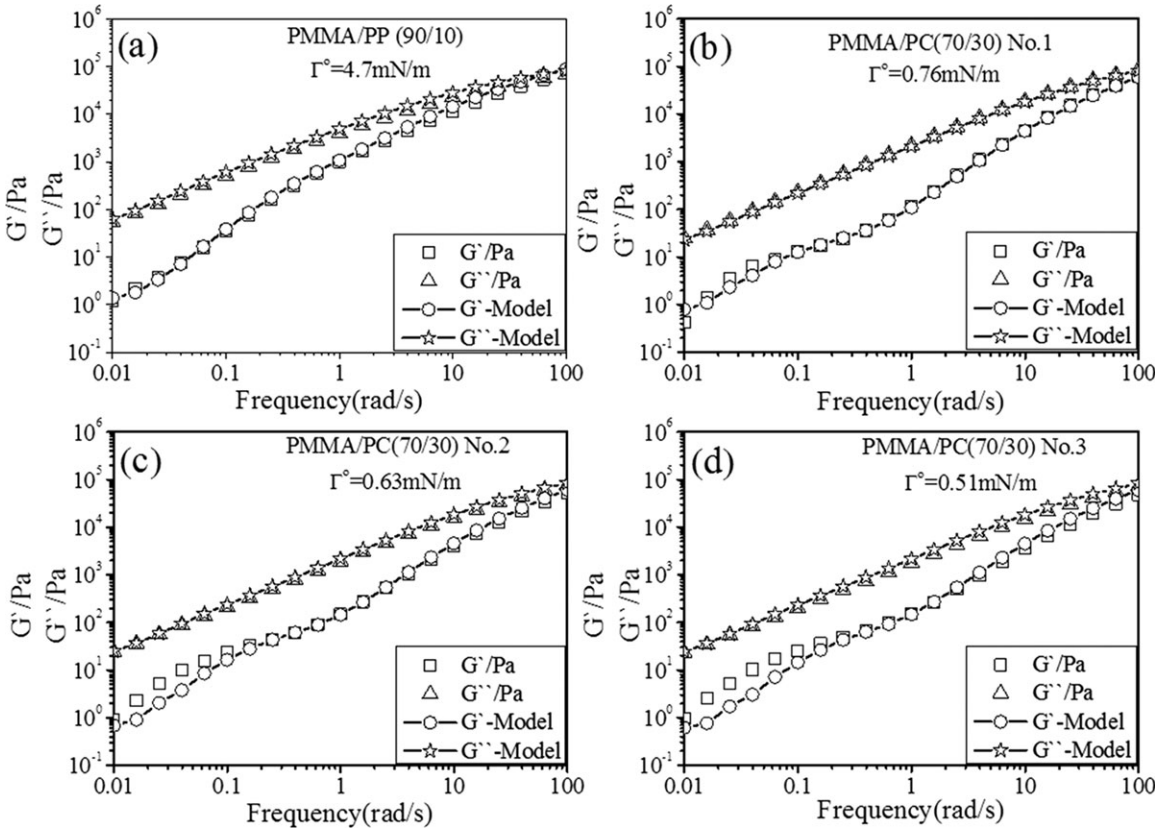

Figure 6. Fit of the Palierne model to the dynamic modulus data.

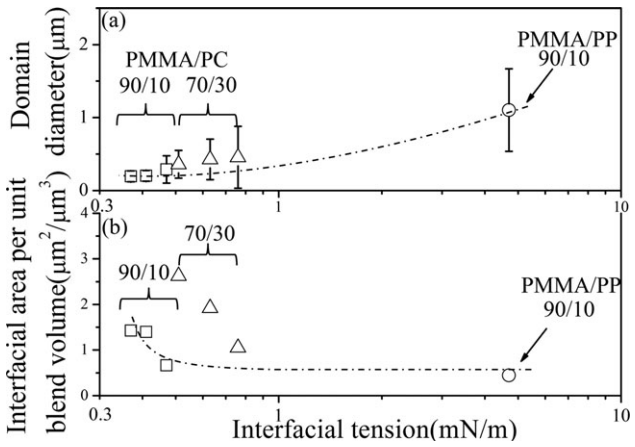

Figure 7. The number average domain diameter, $2 \times \overline{R_d}$ (a) and the interfacial area per unit blend volume, S (b) of PMMA/PP and PMMA/PC blends.

plotted along with interfacial tension, as shown in Figure 7. The disperse domain size in the PMMA/PC blends was smaller and their interfacial areas became larger than those of the PMMA/PP blend. With the increase of copolymer (low-T_d PMMA ratio), the diameter of the PC disperse domain decreased. A better distribution of the PC disperse domain was achieved and larger interfacial areas were produced, as shown in Figure 7(b). Comparing the results of the PMMA/PC blends with a 70/30 weight ratio to those of the PMMA/PC blends with a 90/10 ratio, the PMMA/PC blends with a lower PC ratio exhibited a smaller domain diameter and less interfacial area at all low-T_d PMMA contents.

Cell Morphology of Foamed Blends

Foaming was conducted using 10 MPa of CO_2 at three different temperatures, 60, 80, and 100°C. Under these foaming temperatures, the PMMA phase could be foamed while the PC and PP domains would not be foamed, but they could serve as bubble nucleating agents. Figure 8 presents the SEM micrographs of the foamed PMMA, PMMA/PP, and PMMA/PC blends. The cell density and the cell size were calculated from the SEM micrograph, and the results are illustrated in Figure 9. All the foamed samples possessed spherical cell geometries, but the PC domains were not clearly identified in the cell. This cell morphology of the PMMA/PC blends was quite different from that of the PEG/PS blend foams reported by Taki et al. and that of the PET/PC non-annealed blend foams previously reported by us.[35,12] Sharudin et al. reported that bubble growth dominated at the interface when the interfacial tension was very large.[5] When the polymers in the blend have extremely small interfacial tension, the bubble could grow into one polymer.

By blending PP or PC with high-T_d PMMA, the cell density of the foamed blends became considerably greater than that of the

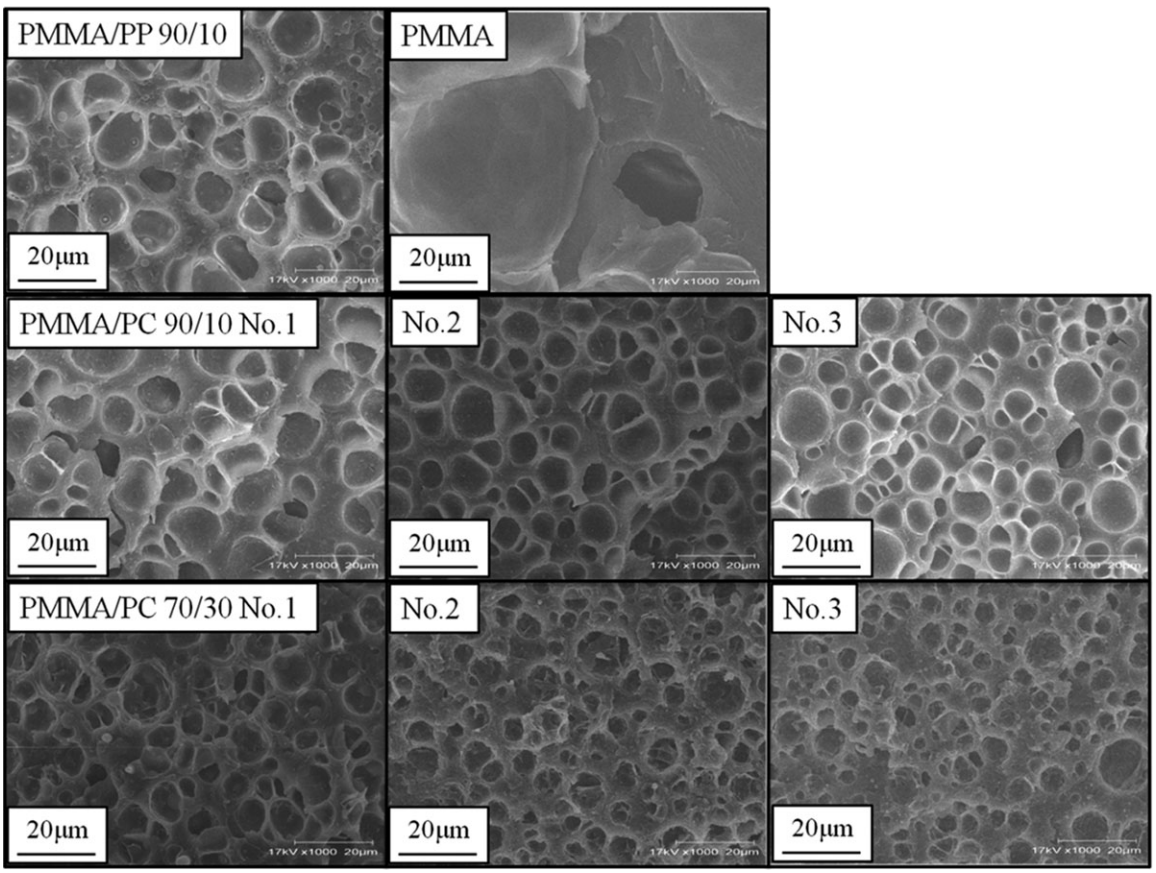

Figure 8. SEM micrographs of PMMA, PMMA/PP and PMMA/PC foamed at 80°C under 10 MPa of CO_2.

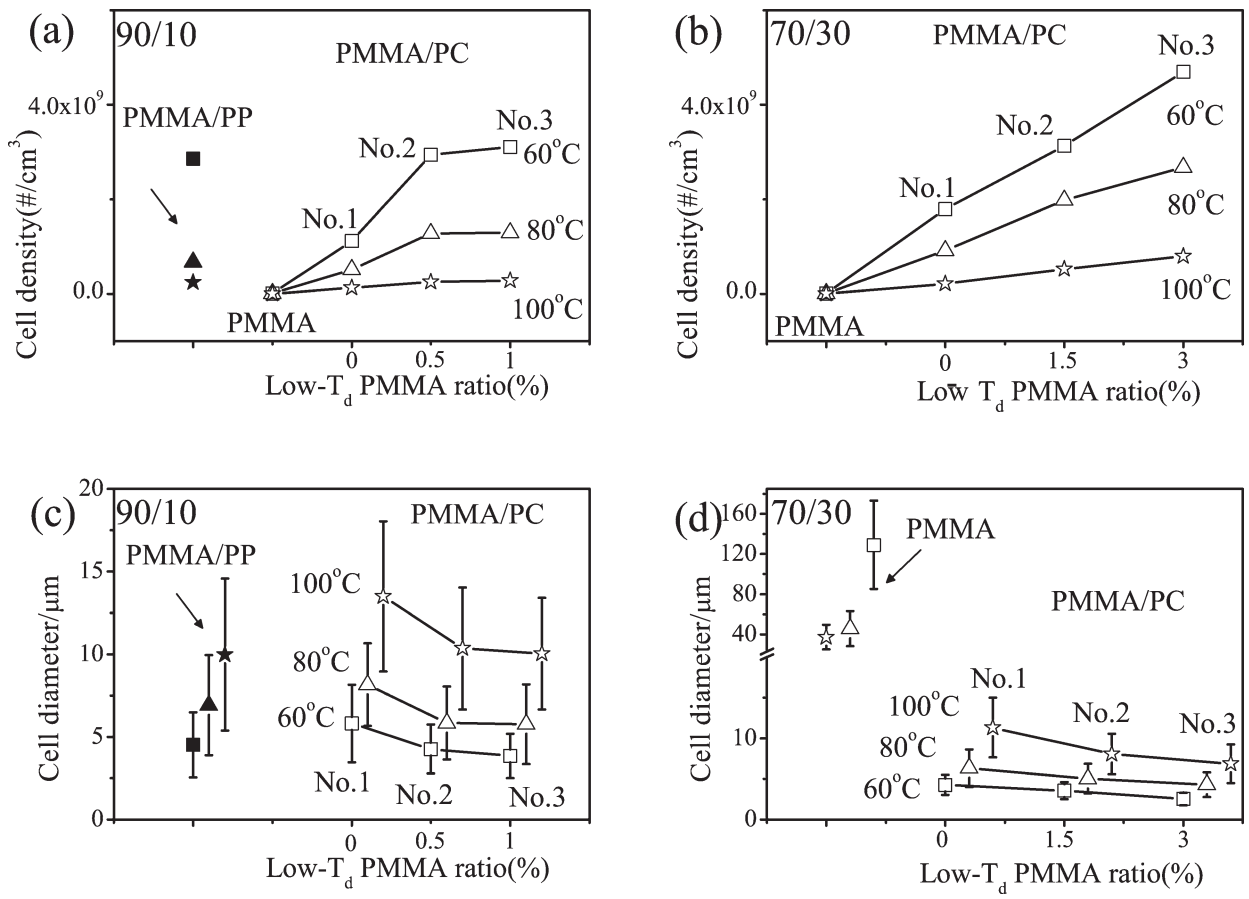

Figure 9. Cell density (a) and (b), and cell size (c) and (d), of the blends foamed at 60, 80, and 100°C.

foamed high-T_d PMMA alone [Figure 9(a,b)]. This result indicates that heterogeneous bubble nucleation became more effective than homogeneous bubble nucleation with the addition of the PP or PC polymer to PMMA. The experimental results also indicate that the cell density increased and the cell size decreased with decreasing foaming temperature. With the decrease of the foaming temperature, the solubility of CO_2 in the polymer blends and the viscoelasticity of the matrix polymer increased. The increase of solubility provided a higher degree of supersaturation, and the increase of viscosity reduced the growth. Both effects served to increase the cell density and reduce the cell size.

In the blend foaming process, heterogeneous bubble nucleation predominantly occurs.[36–38] The cell density becomes a function of the interfacial area and the surface and interfacial tensions, as described by eqs. (20) to (23). Although the exact value of J was difficult to obtain in our study due to the lack of some physical parameter values, the effect of interfacial tension on bubble nucleation could be analyzed from the view of classic heterogeneous bubble nucleation theory. Goel and Bechman reported the surface tension of PMMA with CO_2, γ_A, at 60°C and 10 MPa to be 17 mN m^{-1}.[39] Wong et al. measured the surface tension of PC-CO_2, γ_{B2}, at 240°C and 15 MPa to be 19.5 mN m^{-1}, and Taki et al. measured the surface tension of PP-CO_2, γ_{B1}, at 170°C and 10 MPa to be 12 mN m^{-1}.[40,41] Compared with the surface tensions of those polymers under pressurized CO_2, the interfacial tension of PMMA with PC, γ_{AB2}, is extremely small while the interfacial tension of PMMA with PP, γ_{AB1}, is fairly large. Figure 10 presents two cases of blend foaming (case 1); the interfacial tension between the blend polymers is larger and comparable to those of the surface tensions between polymers and CO_2, and (case 2); the interfacial tension between the blend polymers is considerably less than those of the surface tensions between polymers and CO_2 (case 2). The angles of θ and φ are given in eqs. (20) to (23). In case 1, which is the case of PMMA/PP, less energy is required for bubble nucleation at the interface between polymers. However, in case 2, which is the case of PMMA/PC, more energy is required for bubble nucleation at the interface between two polymers. Consequently, the nucleation at the interface between PMMA and PP is easier than at the PMMA and PC interface.

The number of bubbles per unit interfacial area and the number of bubbles per unit number of domains are shown in Figure 11. The PMMA/PP blend with a high interfacial tension had a greater number of bubbles per unit interfacial area than the PMMA/PC blends. Furthermore, the number of bubbles per unit number of domains decreased with the reduction of interfacial tension because both the nucleation potential at the interface and the domain size decreased. Although the PP domain might not be well-dispersed due to the higher interfacial tension

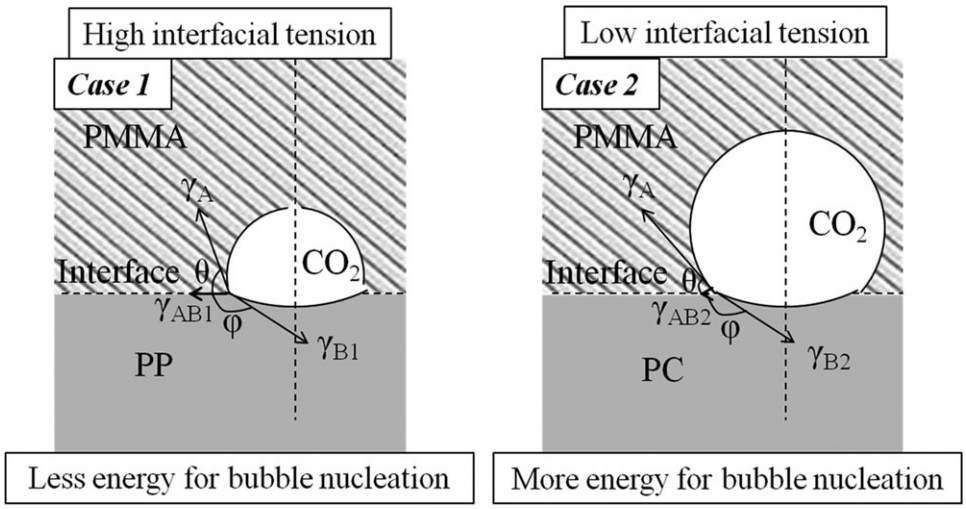

Figure 10. Schematic diagram for the formation of a bubble at the PMMA/PP interface with high interfacial tension (case 1) and the PMMA/PC interface with low interfacial tension (case 2).

between PP and PMMA, the PP domain has greater potential for heterogeneous bubble nucleation than the PC domain. The experimental results indicate that the polymer blends qualitatively follow the classical heterogeneous bubble nucleation mechanism during the foaming process. The interfacial tension has a two-pronged effect on bubble nucleation: the interfacial area can be increased but the heterogeneity is decreased with decreasing interfacial tension. When the interfacial tension is large and the heterogeneity plays a primary role in physical foaming, such as in PMMA/PP, the cell density would decrease with the reduction of interfacial tension between the blended polymers. When the interfacial tension is not considerably great and the interfacial area plays a dominant role, the cell density would increase with the reduction of interfacial tension, as illustrated in Figure 12.

CONCLUSIONS

In this study, the nucleation and growth of bubbles at the interface between blended polymers was investigated by pressure quenched batch foaming. The miscibility of the PC domain with the high-T_d PMMA was controlled by the addition of low-T_d PMMA, which has a low thermal decomposition temperature and serves as a compatibilizer by forming a graft copolymer. The graft copolymer could be produced by melt blending. The copolymer reduces the dissimilarity of the PC domain from the PMMA matrix and reduces the interfacial tension between the two polymers. The reduction of interfacial tension could promote better distribution of the disperse domain, and the bubble nucleation was enhanced by increasing the area of the interface. However, the miscibility at the interface between two blended polymers might affect the bubble nucleation in different manner. When the interfacial tensions were considerably large and were intentionally decreased to improve the dispersibility of the minor phase, the number of bubbles per unit interfacial area and the number of bubbles per unit number of domains could decrease and significantly affect the overall cell density.

The actual performance of the compatibilizer on cell morphology could be determined by compromising the increase of total

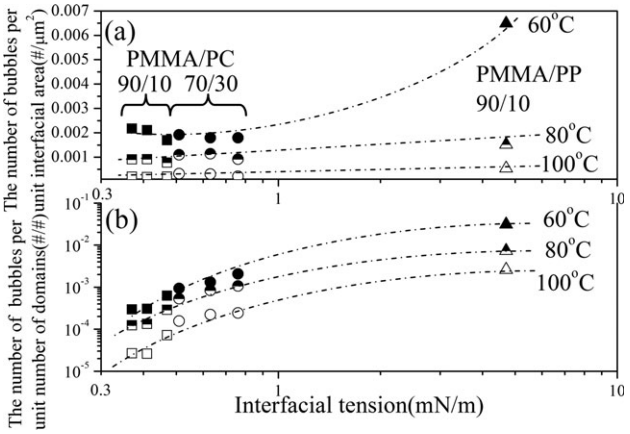

Figure 11. The number of bubbles per unit interfacial area (a) and the number of bubbles per unit number of domains (b) at different foaming temperatures: 60, 80, and 100°C.

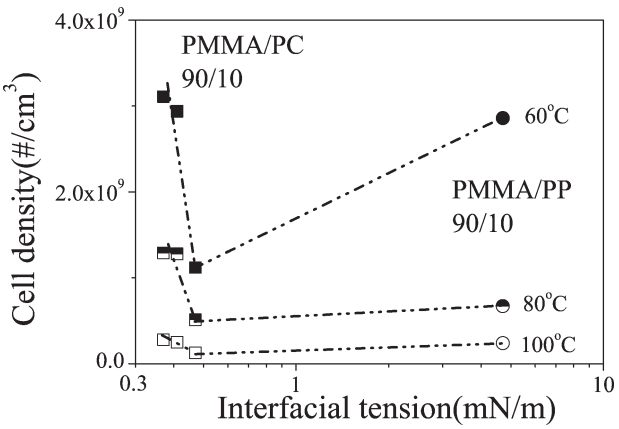

Figure 12. Cell density as a function of interfacial tension at different foaming temperatures: 60, 80, and 100°C.

area of heterogeneous interface and the decrease of bubble nucleation ability per unit interfacial area. In this study, the true number of bubble nuclei could not be observed due to limitations of the SEM observation. However, this study clearly reveals an aspect of the effect of the bubble nucleating agent on the resulting cell morphology.

REFERENCES

1. Klempner, D.; Frisch, K. C. In Handbook of Polymeric Foams and Foam Technology; Oxford University Press: New York, **1991**; Chapter 1, p 2.
2. Ruckdaschel, H.; Gutmann, P.; Altstadt, V.; Schmalz, H.; Muller, A. H. E. *Adv. Polym. Sci.* **2010**, *227*, 199.
3. Colton, J. S.; Suh, N. P. *Polym. Eng. Sci.* **1987**, *27*, 485.
4. Colton, J. S.; Suh, N. P. *Polym. Eng. Sci.* **1987**, *27*, 493.
5. Sharudin, R. W.; Nabil, A.; Taki, K.; Ohshima, M. *J. Appl. Polym. Sci.* **2010**, *119*, 1042.
6. Park, C. B.; Lee, P. C.; Wang, J.; Padareva, V. *Cell. Polym.* **2006**, *25*, 1.
7. Siripurapu, S.; DeSimone, J. M.; Khan, S. A. Spontak, R. J. *Macromolecules* **2005**, *38*, 2271.
8. Spitael, P.; Macosko, C. W.; McClurg, R. B. *Macromolecules* **2004**, *37*, 6874.
9. Zhai, W.; Wang, H.; Yu, J.; Dong, J.; He, J. *J. Polym. Sci. Part B: Polym. Phys.* **2008**, *46*, 1641.
10. Ruckdaschel, H.; Sandler, J. K. W.; Altstadt, V.; Retting, C.; Schmalz, H.; Abetz, V.; Muller, A. H. E. *Polymer* **2006**, *47*, 2772.
11. Baker, W. E.; Scott, C. E.; Hu, G. H. In Reactive Polymer Blending; Hanser Gardner Publications, Inc.: Cincinnati, **2001**; Chapter 3, p 53.
12. Gong, P.; Ohshima, M. *J. Polym. Sci. Part B: Polym. Phys.* **2012**, *50*, 1173.
13. Kyu, T.; Lim, D. *J. Chem. Phys.* **1990**, *92*, 3951.
14. Kyu, T.; Saldanha, J.M. *J. Polym. Sci. Part B: Polym. Phys.* **1990**, *28*, 97.
15. Rabeony, M.; Hseih, D. T.; Garner, R. T.; Peiffer, D. G. *J. Chem. Phys.* **1992**, *97*, 4050.
16. Marchese, P.; Celli, A.; Fiorini, M. *Macromol. Chem. Phys.* **2002**, *203*, 695.
17. Montaudo, G.; Puglisi, C.; Samperi, F. *J. Polym. Sci. Part A: Polym. Chem.* **1998**, *36*, 1873.
18. Ko, C. C.; Kyu, T.; Smith, S. D. *J. Polym. Sci. Part B: Polym. Phys.* **1995**, *33*, 517.
19. Cole, P. J.; Cook, R. F.; Macosko, C. W. *Macromolecules* **2003**, *36*, 2808.
20. Asthana, H.; Jayaraman, K. *Macromolecules* **1999**, *32*, 3412.
21. Kohlhoff, D.; Ohshima, M. *Macromol. Mater. Eng.* **2011**, *296*, 770.
22. Porter, R. S.; Wang, L. H. *Polymer* **1992**, *33*, 2019.
23. Marin, N.; Favis, B. D. *Polymer* **2002**, *43*, 4723.
24. Palierne, J. F. *Rheol. Acta.* **1990**, *29*, 204.
25. Scholz, P.; Froelich, D.; Muller, R. *J. Rheol.* **1989**, *33*, 481.
26. Graebling, D.; Muller, R.; Palierne, J. F. *Macromolecules* **1993**, *26*, 320.
27. Blander, M. *Adv. Colloid Interface Sci.* **1979**, *10*, 1.
28. Kyu, T.; Ko, C. C.; Lim, D. S.; Smith, S. D.; Noda, I. *J. Polym. Sci. Part B: Polym. Phys.* **1993**, *31*, 1641.
29. Debier, D.; Devaus, J.; Legras, R. *J. Polym. Sci. Part A: Polym. Chem.* **1995**, *33*, 407.
30. Kim, W. N.; Burns, C. M. *Macromolecules* **1987**, *20*, 1876.
31. Larson, R. G. The Structure and Rheology of Complex Fluids; Oxford University Press: New York, **1999**; Chapter 9, p 414.
32. Wu, S. *Polym. Eng. Sci.* **1987**, *27*, 335.
33. Virgilio, N.; Desjardins, P.; L'Esperance, G.; Favis, B. D. *Macromolecules* **2009**, *42*, 7518.
34. Moussaif, N.; Jerome, R. *Macromol. Symp.* **1999**, *139*, 125.
35. Taki, K.; Nitta, K.; Kihara, S. I.; Ohshima, M. *J. Appl. Polym. Sci.* **2005**, *97*, 1899.
36. Reyes-Lozano, C. A.; Gudino, P. O.; Gonzalez-Nunez, R; Rodrigue, D. *J. Cell Plast.* **2011**, *47*, 153.
37. Zepeda, S. C.; Gonzalez-Nunez, R.; Rodrigue, D. *J. Cell Plast.* **2006**, *42*, 469.
38. Herrera, T.E.; Zepeda, S.C.; Gonzalez-Nunez, R.; Rodrigue, D. *J. Cell Plast.* **2005**, *41*, 417.
39. Goel, S. K.; Bechman, E. J. *Polym. Eng. Sci.* **1994**, *34*, 1137.
40. Wong, A.; Leung, S. N.; Li, G. Y. G.; Park, C. B. *Ind. Eng. Chem. Res.* **2007**, *46*, 7107.
41. Taki, K.; Murakami, T.; Ohshima, M. Proceeding of the Asian Workshop of Polymer Processing (AWPP); Japan Society of Polymer Processing: Singapore, **2002**.